

Single-Shot Multi-Person 3D Body Pose Estimation From Monocular RGB Input

Dushyant Mehta¹, Oleksandr Sotnychenko¹, Franziska Mueller¹,
Weipeng Xu¹, Srinath Sridhar², Gerard Pons-Moll¹ and Christian Theobalt¹

¹Max Planck Institute For Informatics, Germany ²Stanford University, USA

Abstract

We propose a new efficient single-shot method for multi-person 3D pose estimation in general scenes from a monocular RGB camera. Our fully convolutional DNN-based approach jointly infers 2D and 3D joint locations on the basis of an extended 3D location map supported by body part associations. This new formulation enables the readout of full body poses at a subset of visible joints without the need for explicit bounding box tracking. It therefore succeeds even under strong partial body occlusions by other people and objects in the scene. We also contribute the first training data set showing real images of sophisticated multi-person interactions and occlusions. To this end, we leverage multi-view video-based performance capture of individual people for ground truth annotation and a new image compositing for user-controlled synthesis of large corpora of real multi-person images. We also propose a new video-recorded multi-person test set with ground truth 3D annotations. Our method achieves state-of-the-art performance on challenging multi-person scenes.

1. Introduction

Single-person pose estimation, both 2D and 3D, from monocular RGB input is a challenging and widely studied problem in vision [3, 2, 25, 26, 6, 9, 21, 29]. It has many practical applications, for instance in activity recognition, human-machine interaction, or content creation for graphics. There has been much progress in single person 2D pose estimation, and some methods for more challenging 2D multi-person pose estimation were shown. However, work on 3D pose estimation methods has been mostly restricted to single unoccluded subjects. Many natural human activities take place in groups with multiple persons and in cluttered scenes. Monocular input with multiple people therefore not only exhibits self-occlusions of the body, but also strong inter-person occlusions or occlusions by objects, which add to the already difficult under-constrained problem of inferring 3D pose from monocular RGB input.

Further, it is very hard to manually annotate or compute 3D ground truth for multi-person training image sets. Consequently, only very few methods have approached this more general 3D multi-person pose estimation problem [36], and it is still largely unsolved.

This paper proposes a new learning-based method to estimate 3D pose of multiple persons in general scenes from monocular input, as well as a new way of creating realistic training data at a large scale. While there are many single-person datasets with ground truth 3D annotations, there are no multi-person datasets that contain realistic human-human interaction with person and background diversity. Computing, let alone manually annotating, such data at scale is difficult because of occlusions and the sheer number of annotations required. Previous approaches to the dataset problem [36] propose using 2D pose data augmented with 3D poses from motion capture datasets, or find 3D consistency in 2D part annotations from a multi-view images [40]. In this work, we transform the MPI-INF-3DHP single person dataset [25] into the first multi-person set with complex interactions, ground truth 3D, and real images of people. This dataset, which we call *MuCo-3DHP*, is created by compositing multiple 2D person images with ground truth 3D pose from multi-view capture, and varying backgrounds into a single frame. This allows us to controllably generate combinatorially large amounts of real image data for training. There are also very few multi-person test datasets with ground truth annotation [10] showing more than 2 people. We therefore captured a new multi-person 3D test set with indoor and outdoor scenes, challenging occlusions and interactions, and varying backgrounds, to evaluate our method. All datasets will be made publicly available.

Recent attempts at addressing the 3D multi-person pose estimation problem [36] employ a detection framework to obtain bounding box proposals of each person. This complicates reasoning under occlusion, in strong inter-person interaction, and furthermore induces a runtime penalty when scaling to many persons in a scene. We propose a *sin-*

This work was funded by the ERC Starting Grant project CapReal (335545). We would also like to thank Hyeongwoo Kim and Eldar Insafutdinov for their assistance in the project.

gle shot DNN-based method to extract multi-person 3D pose. It reasons about all people in a scene jointly and does not require explicit bounding box detection proposals [36] which may be unreliable under strong occlusions and expensive to compute in dense multi-person scenes. Our fully-convolutional method infers 2D and 3D joint locations together. It uses an enhanced 3D location map representation [26] specially tailored to the multi-person case. It allows the readout of a full 3D pose at a detected 2D torso root location, and articulation refinement at selected other joint locations further down the kinematic chain, and thus can jointly infer full 3D pose of multiple people even under partial occlusion. Our main insight is that not all body parts need be visible to make a complete pose inference, but if limbs are visible, they can be used to improve the pose readout from the main torso. Quantitative evaluation shows that estimating 3D pose at the torso root and then refining it at the limbs produces much better pose estimates than other approaches. To sum up, we contribute:

- A learning-based single-shot multi-person pose estimation method that predicts both 2D and 3D joint locations without the need for bounding box extraction. Our method is tailored for scenes with occlusion by objects or other people.
- The first multi-person dataset of real person images with 3D ground truth that contains complex inter-person occlusions and motion. Our compositing approach enables us to synthesize large amounts of data under user control, for learning based approaches.
- A real in-the-wild test set for evaluating multi-person 3D pose estimation methods that contains challenging multi-person interactions, occlusions, and motion.

2. Related Work

In this review, we focus on most directly related work, namely estimating the pose of *multiple people in 2D* or *single person in 3D* from monocular RGB. [37] provide a more comprehensive review. With the exception of [36] ours is the first method for monocular *multiple person 3D pose estimation*.

Multi-Person 2D Pose Estimation: A common approach for multiple people 2D pose estimation is to first detect single persons and then predict the 2D pose for each detection [32, 11, 42, 15, 30]. Unfortunately, these methods fail when the detectors fail which is likely to happen in multiple people scenarios with strong occlusions. Hence, a body of work first localizes the joints of each person with CNN-based detectors and then find the correct association between joints and subjects in a post-processing step. The associations are obtained by solving a fully connected graph in [31]. This involves solving an NP-hard integer linear program which easily takes hours per image. The

work of [13] improves the performance of [31] by including image-based pairwise terms and using stronger detectors based on ResNet [12]. This approach takes minutes instead of hours but it is still computationally very expensive and can only handle a limited number of proposals. Cao *et al.* [7] detect joint locations and Part Affinity Fields (PAFs), which are 2D vectors indicating the direction of bones in the skeleton. By using PAFs and greedy part association they achieve real time multi-person 2D pose estimation results. Others simultaneously predict joint locations and their associations [28] using a stacked-hour glass CNN [29].

Single-Person 3D Pose Estimation: Many monocular single person 3D methods show good performance on standard benchmarks, such as [14, 38]. Many methods train a discriminative predictor that regresses directly to 3D poses [4]. However, they often do not generalize well to natural scenes with varied poses, appearances, backgrounds and occlusions. This is due to the fact that most aforementioned 3D datasets are restricted to indoor setups with limited backgrounds. The advent of large real world image datasets with 2D annotations made 2D monocular pose estimation in the wild remarkably accurate. Annotating images with 3D poses is much harder. Hence, recent works have focused on leveraging 2D image datasets for 3D human pose estimation. Some works split the problem in two: they first estimate 2D joints and then lift them to 3D. In the seminal works of [44, 41] they achieve that by reasoning about kinematic depth ambiguities; in [8, 49] they match detected 2D joints with a database of 3D poses; in [27] they regress pose from a 2D joint distance matrix. Another option is to exploit pose and geometric priors for lifting [51, 1, 39, 16]; in [24] they train a feed forward network to directly predict 3D pose from 2D joints; in [5, 20] they fit a recently released human body model [23] to 2D detections.

Other works leverage the features learned by a 2D pose estimation CNN for 3D pose estimation, assuming that features discriminative for 2D estimation should be useful in the 3D case as well. For example, in [45] they learn to merge features from a 2D joint prediction network and a 3D joint prediction network. Another approach is to train a network with separate 2D and 3D losses for the different data sources [34, 50, 43]. The advantage of such methods is that they can be trained end to end. A simpler yet very effective approach is to refine a network trained for 2D pose estimation for the task of 3D pose estimation [26, 25]. A major limitation of methods that rely on 2D joint detections directly or for bounding boxes is that they easily fail under body occlusion or if some of the 2D detections are incorrect, both of which are common in multi-person scenes. In contrast, our approach is more robust to occlusions since the complete global 3D pose can be read out at the first non-occluded location of pelvis, spine or neck. As shown in [26], 3D joint prediction works best when the prediction



Figure 1. Examples from MuCo-3DHP dataset, created through compositing MPI-INF-3DHP [25] data. (Top) composited examples without appearance augmentation, (bottom) with BG and clothing augmentation. The last two columns show rotation and scale augmentation, and truncation with the frame boundary.

is centered at the 2D joint of interest.

Multi-Person 3D Pose Estimation: To our knowledge, only Rogez *et al.* [36] tackle multi-person 3D pose estimation from one image. Their method uses a pipeline consisting of localization, classification and regression. They first identify proposals of bounding boxes likely to contain a person using [35]. Instead of regressing to pose directly, they then classify the bounding box into a set of K-poses, which is similar to [33]. These poses are scored by a classifier and refined using a regressor. All three components share the convolutional feature layers and are trained jointly. However, the method still reasons using bounding boxes internally and produces multiple proposals per subject that need to be accumulated and fused. Results with severe person-person occlusions are not shown. In contrast, our approach uses a fully-convolutional network, and produces multi-person 2D joint locations and 3D location maps in a single shot, from which the 3D pose can be inferred after grouping the 2D joint detections by people. **3D Pose Datasets:** Existing pose datasets are either for a single person in 3D [14, 38, 47, 48, 25] or multi-person with only 2D pose annotations [2, 22]. One exception is the MARCOI dataset [10] that features 5 sequences but contains only 2 persons simultaneously and there are no close interactions. We choose to leverage the person segmentation masks available in MPI-INF-3DHP [25] to generate annotated multi-person 3D pose images of real people through compositing. The ground truth annotations for each person were obtained through multiview marker-less motion capture [25]. Then we compose images of multiple people by stacking layers with different people simulating people-people occlusions, see Section 3.

3. Multi-Person Dataset

As discussed, single person image data sets with 3D pose annotation at scale and with sufficient appearance diversity were generated. Previous work used a combination of transfer learning [25, 50] and appearance augmentation [25] with



Figure 2. Sample frames from the proposed multi-person test set. Ground truth reference is available for up to 3 subjects in the scene (shown projected on to the image on the left). The set covers a variety of scene settings, activities and clothing.

marker-based [14] and marker-less [25] indoor motion capture. At first it may seem trivial to extend these concepts to the multi-person case, i.e., use a combination of in-the-wild multi-person 2D pose data [2, 22] and multi-person multi-view motion capture for 3D annotation. However, multi-person 3D motion capture under strong occlusions and difficult interactions is still challenging even for commercial multi-view systems. In such scenes, manual pose correction is often needed, and 3D accuracy is thus constrained. This severely limits the scale at which real multi-person data can be captured and processed.

Hence, we employ multi-view marker-less motion capture only to create the 20 sequences of the first expressive in-the-wild test set for multi-person 3D pose estimation. For the much larger training set MuCo-3DHP, however, we resort to a new compositing and augmentation scheme that leverages the single-person image data of real people in MPI-INF-3DHP[25] to composite an arbitrary number of real multi-person interaction images with captured ground truth 3D under user control.

3.1. MuCo-3DHP: Compositing-Based Training Set

The recently released MPI-INF-3DHP [25] single person 3D pose dataset provides marker-less motion capture based annotations for real images of 8 subjects, each captured with 2 clothing sets, using 14 cameras with different elevations. We leverage the person segmentation masks to create per-camera composites with 1 to 4 subjects, with frames randomly selected from the 8×2 sequences available per camera. Since we have ground truth 3D skeleton pose for each video subject in the same space, compositing can be done in a 3D-aware way, resulting in correct depth ordering and overlap of the composited subjects, without any interpenetration of 3D bounding boxes. We refer to this composited training set as the **Multiperson Composited 3D Human Pose dataset**. Example composites are shown in Fig.1. The compositing process results in plausible images covering a range of simulated inter-person overlap and activity scenarios. User-control over desired pose and occlusion distri-

butions during synthesis, and further FG/BG augmentation using the masks provided with MPI-INF-3DHP, is possible. For details on further processing applied to MuCo-3DHP dataset while training, please refer to the supplementary document. Even though the synthesized composites may not simulate all fine-grained aspects of human-human interaction fully, our approach trained on these data generalizes well to real world scenes shown in our test set.

3.2. Test Set

We provide a new filmed, not composited, multi-person test set comprising 20 general real world scenes with ground truth 3D pose for up to three subjects obtained with a multi-view marker-less motion capture system [46]. The set covers 5 indoors and 15 outdoor settings, with stationary and moving backgrounds, trees, office buildings, road, people, vehicles, and other distractors in the background. Additionally, some of the outdoor footage have challenging elements, *e.g.*, drastic illumination changes, and lens flare. The indoor sequences use footage at 2048×2048 px resolution at 30fps, outdoor sequences were captured with GoPros at 1920×1080 px resolution at 60fps. The test set consists of >8000 frames, split among the 20 sequences, with 8 subjects, in a variety of clothing styles, poses, interactions, and activities. A key feature is that the test sequences do not resemble the training sequences, and include real interaction scenarios.

Evaluation Metric: We use the robust *3DPCK* evaluation metric proposed in [25]. It treats a joint’s prediction as correct if it lies within a 15cm ball centered at the ground truth joint location, and is evaluated for the common minimum set of 14 joints marked in green in Figure 3. We report the *3DPCK* numbers per sequence, averaged over the subjects for which GT reference is available. Occluded joints or subjects are not excluded from the evaluation.

4. Method

Location Maps: In previous work [26] it has been observed that 3D pose inference can be linked more strongly to image evidence by inferring 3D joint positions at the respective 2D joint pixel locations using a fully convolutional neural network. This forces the network to focus on the image evidence around the 2D joint when inferring its 3D counterpart. This is achieved using *location maps*. A location map for a joint is a 2D feature channel with each of its 2D pixel locations storing the most likely x , y , or z coordinate for that joint, conditional on the 2D prediction for that joint being at that 2D pixel location. For an input image of size $W \times H$, $3n$ location maps (each of size $W/4 \times H/4$) are used to store the 3D location of all n joints. Location maps are trained to produce reliable 3D predictions at image locations where 2D joints are detected. Hence, at test time, the 3D joint location is *read out* at the corresponding 2D de-

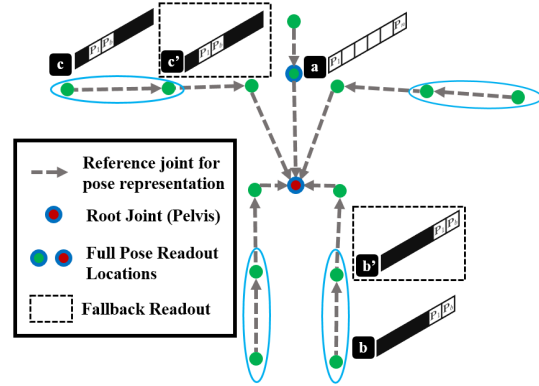


Figure 3. We represent human body pose as a hierarchical skeleton with 17 joints (of which only 15 are shown here for clarity). Our location maps store the 3D joint locations of the whole body at the 2D position of the neck and the pelvis, and limb-specific pose at all limb joints (blue ovals). During 3D pose inference, we first obtain the complete 3D pose from the neck/pelvis joint (a). We then refine it by replacing the limb sub-pose with the readout from a joint representative of that limb (b, c). In case the representative joint is occluded, we fall back to a joint further up in the skeleton hierarchy (b’, c’).

tection. Per-joint location inference as proposed in [26], enables full 3D pose inference only if the person is completely visible. It therefore breaks down when joints are occluded, which happens often in general scenes. Self-occlusions, person-person occlusions, occlusions by objects, and body truncation at frame boundaries are common in multiple persons scenes. In the following, we detail our formulation and our solution to handle these challenges.

4.1. Formulation

Given a monocular RGB image \mathcal{I} , we seek to estimate the 3D pose $\mathcal{P} = \{\mathbf{P}_i\}_{i=1}^m$ for each of the m persons in the image. Here, $\mathbf{P}_i \in \mathbb{R}^{3n}$ describes the 3D locations of the n ($n = 17$) body joints of person i . The joint locations are encoded relative to their reference joints, marked with arrows in Figure 3. We make use of 2D joint *heatmaps* $\mathcal{H} = \{\mathbf{H}_j\}_{j=1}^n$ predicted by our network to encode the detection confidence of each joint type j in the image. Additionally, we predict *part affinity fields* $\mathcal{A} = \{\mathbf{A}_k\}_{k=1}^{2n}$ which encode a 2D vector field for each body part denoting the direction pointing from the parent joint to its child [7]. This facilitates association of 2D detections to person identities when there are multiple people in the scene. The 3D locations of each joint j that our network predicts are encoded in the *location maps* denoted by $\mathcal{X} = \{\mathbf{X}_j\}_{j=1}^n$, $\mathcal{Y} = \{\mathbf{Y}_j\}_{j=1}^n$, and $\mathcal{Z} = \{\mathbf{Z}_j\}_{j=1}^n$, where $\mathbf{X}_j, \mathbf{Y}_j, \mathbf{Z}_j \in \mathbb{R}^{w \times h}$, $w = W/4$, and $h = H/4$. Note that we predict a fixed number of maps (n heatmaps, $3n$ location maps, and $2n$ part affinity fields) irrespective of the number of persons in the scene making our method scale without additional processing.

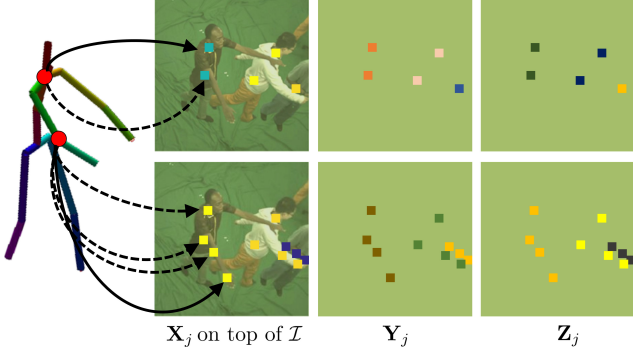


Figure 4. During training, the location maps for each person’s joints are defined by specifying their 3D position at multiple 2D joint locations (columns 1–3). For instance, the 3D position of the neck (red dot in skeleton) can be read out either at the pelvis or at the neck 2D locations. The 3D position of the left elbow (red dot in skeleton) can be read out at the wrist, pelvis, neck, or elbow 2D locations. Dotted lines indicate secondary read out priority in case the primary read out joint location is occluded (see Algorithm 1). Note that the 3D location of multiple persons are encoded into the same map and no additional channels are needed.

Occlusion-Robust Location Maps: At the core of our method is a carefully designed encoding of pose for multiple persons which we call *Occlusion-Robust Location Maps* (ORLM). ORLMs have two special features: (1) they support a special *read out scheme* (see Section 4.2) that makes our method robust to partial occlusions of the body, (2) they encode the pose of multiple persons without needing a variable number of outputs.

To support our special read out scheme, we decompose the body into torso, four limbs, and head (see Figure 3). We denote as *full pose* the vector $\mathbf{P} \in \mathbb{R}^{3n}$ containing all joint locations. We denote as *limb pose* the part of the pose parameters corresponding to the limb, e.g., the limb-pose of the left arm is a vector of 6 parameters consisting of two 3D vector offsets: shoulder–elbow, and elbow–wrist. Given this decomposition, the ORLM are trained such that (see Figure 4):

- At the root and neck location the full pose can be read out, and
- At the wrist, elbows, ankles and knees location the corresponding limb pose can be read out.

Notice that ORLM have redundancy built in to better deal with occlusions at inference time. For instance, the 3D location of the left elbow can be read out at four different pixel locations, namely, at the neck, root, wrist and the elbow 2D location (see Figure 4). Therefore, if a particular joint is occluded in the image we read the pose information at a different joint as explained in Section 4.2.

While in the original formulation location maps encode the 3D pose for only a single person, ORLM encode the 3D pose for all persons jointly without adding more channels.

As shown in Figure 4, during training, we encode the the full 3D pose of multiple persons within the location maps. This ensures efficient pose inference even when multiple persons are visible without needing variable outputs.

Algorithm 1 3D Pose Inference

```

1: Given:  $\mathcal{P}^{2D}, \mathcal{C}^{2D}, \mathcal{X}, \mathcal{Y}, \mathcal{Z}$ 
2: for all  $i \in (1..m)$  do
3:   if  $\mathbf{C}_i^{2D}[k] > thresh, k \in \{pelvis, neck\}$  then
4:     Person  $i$  is detected
5:     for all joints  $j \in (1..n)$  do
6:        $rloc = \mathbf{P}_i^{2D}[k]$ 
7:        $\mathbf{P}_i[:, j] = \text{READLOCMAP}(j, rloc)$ 
8:       for all joints  $a$  in  $l, l \in \{limbs, head\}$  do
9:         if  $\text{ISVALIDREADOUTLOC}(i, a)$  then
10:           $rloc = \mathbf{P}_i^{2D}[a]$ 
11:          for all joints  $b \in \text{limb } l$  do
12:             $\mathbf{P}_i[:, b] = \text{READLOCMAP}(b, rloc)$ 
13:          break
14:       else
15:         No person detected
16: function  $\text{READLOCMAP}(\text{joint } j, \text{2DLocation } rloc)$ 
17:    $rloc = rloc / locMap\_scale\_factor$ 
18:    $\mathbf{P} = (\mathbf{X}_j[rloc], \mathbf{Y}_j[rloc], \mathbf{Z}_j[rloc])$ 
19:   return  $\mathbf{P}$ 
20: function  $\text{ISVALIDREADOUTLOC}(\text{person } i, \text{joint } j)$ 
21:   if  $(\mathbf{C}_i^{2D}[j] > 0)$  then
22:     return  $\text{ISISOLATED}(i, j)$ 
23:   else
24:     return 0
25: function  $\text{ISISOLATED}(\text{person } i, \text{joint } j)$ 
26:    $\mathcal{M} = p, p \in (1..m), p \neq i$ 
27:    $lt = \text{limb\_type}(j)$ 
28:    $isol = 1$ 
29:   for all person  $\tilde{i} \in \mathcal{M}$  do
30:     for all joints  $\tilde{j}$  with  $\text{limb\_type}(\tilde{j}) == lt$  do
31:       if  $\|\mathbf{P}_{\tilde{i}}^{2D}[\tilde{j}] - \mathbf{P}_i^{2D}[j]\|_2 < isoThresh$  then
32:          $isol = 0$ 
33:       break
34:   return  $isol$ 

```

4.2. Pose Inference

3D pose inference of multiple people from ORLM is predicated on successful 2D joint location inference and association.

2D Pose Inference: We infer 2D joint locations $\mathcal{P}^{2D} = \{\mathbf{P}^{2D}_i\}_{i=1}^m, \mathbf{P}^{2D}_i \in \mathbb{R}^{2 \times n}$ and joint detection confidences $\mathcal{C}^{2D} = \{\mathbf{C}^{2D}_i\}_{i=1}^m, \mathbf{C}^{2D}_i \in \mathbb{R}^n$ for each person i in the image. Explicit 2D joint-to-person association is done with the predicted *heatmaps* \mathcal{H} and *part affinity fields* \mathcal{A} using the approach of Cao *et al.* [7].

3D Pose Inference with ORLM : We use the 2D body joint locations \mathcal{P}^{2D} and the body joint detection confidences \mathcal{C}^{2D} to infer the 3D pose of all persons in the scene. Algorithm 1 describes the 3D pose inference process which is also visually explained in Figure 3. Since occlusions occur, the naive approach reading of 3D joint locations at 2D detections completely fails. To that end, we propose two strategies to handle occlusions: (1) *read out priority* and (2) *2D joint validation*.

Read Out Priority: By virtue of the ORLM we can read out joint predictions at different pixel locations which makes us robust to occlusions. Let us denote as *extremity joints*: the wrists, and ankles, and as *middle-joints*: the elbows and knees. The neck and the root joint 2D detections are usually reliable, these joints are most often not occluded and lie in the middle of the body. Therefore, we start reading the full pose at the neck location. If the neck is *invalid* (as defined below) then the full pose is read at the pelvis. If both joints are *invalid* we consider that person is not visible in the scene and we do not predict their pose. While robust, full poses read at the pelvis and neck tend to be closer to the average pose in the training data. Therefore, for every limb, we continue by reading out the limb pose at the extremity joint. If the extremity joint is valid, the limb pose replaces the corresponding elements of the full pose. If the extremity joint is invalid we try to read out the limb pose at the middle joint. If the middle joint is valid the limb pose replaces the corresponding elements of the full pose. If the middle joint is also invalid, the prediction for the limb pose will come from the neck/pelvis full pose read out. The procedure is illustrated in Figure 3. This inference strategy with priority makes us robust to occlusions.

2D Joint Validation: We check a selected 2D joint and mark it as *valid* if it satisfies 2 conditions: (1) is unoccluded, *i.e.* has confidence value higher than a threshold, and (2) is sufficiently far away from similar joints on another person. If both conditions are satisfied, we lookup the corresponding 3D pose based on the read out priority. Otherwise, we fall back to a limb joint higher up in the hierarchy (*e.g.*, ankle for leg, elbow for arm) until the above conditions are satisfied. The redundancies and fall backs incorporated in our pose inference algorithm ensure reliable pose estimation in the presence of strong inter-person occlusions. Even if none of the limb joints are visible, we can still estimate a reasonable 3D pose based solely on the torso readout.

4.3. Network Details

Our network is based on ResNet-50 [12]. The original architecture is preserved till *res4f*, after which we split it into two—a *2DPose+Affinity* stream and a *3DPose* stream. Architectural specifics of the two streams may be found in the supplemental document. The *2DPose+Affinity* stream predicts the 2D heatmaps \mathcal{H}_{COCO} for the MS-COCO body

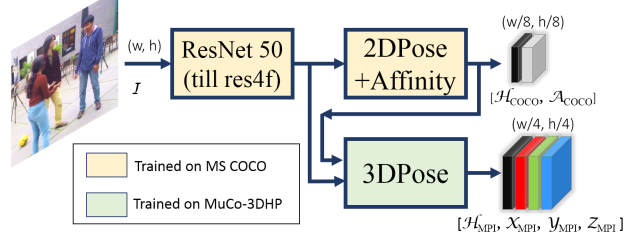


Figure 5. The network architecture with *2DPose+Affinity* branch predicting the 2D *heatmaps* \mathcal{H}_{COCO} and *part affinity maps* \mathcal{A}_{COCO} with a spatial resolution of $(W/8, H/8)$, and *3DPose* branch predicting 2D *heatmaps* \mathcal{H}_{MPI} and location maps $\mathcal{X}_{MPI}, \mathcal{Y}_{MPI}, \mathcal{Z}_{MPI}$ with a spatial resolution of $(W/4, H/4)$, for an input image with resolution (W, H) .

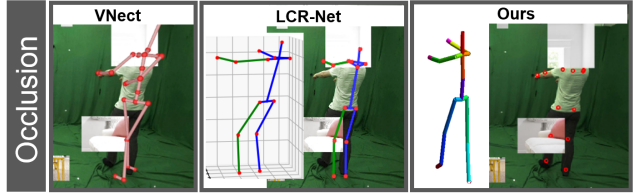


Figure 6. Test for robustness to occlusion using textured synthetic rectangles overlaid on the TS1 sequence from MPI-INF-3DHP.

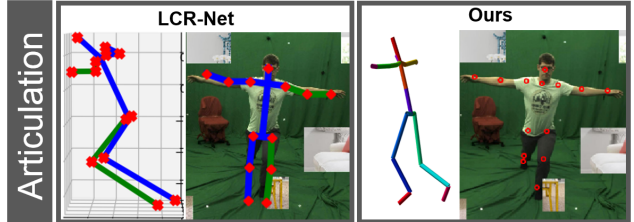


Figure 7. Qualitative evaluation of the extent of articulation of LCR-net and Our method. 3D pose viewed from the side.

joint set, and part affinity fields \mathcal{A}_{COCO} .

The *3DPose* stream predicts 3D pose location maps $\mathcal{X}_{MPI}, \mathcal{Y}_{MPI}$ and \mathcal{Z}_{MPI} , as well as 2D heatmaps \mathcal{H}_{MPI} for the VNect (MPI-INF-3DHP [25]) joint set, which has some overlap with the MS-COCO joint set, but does not include facial keypoint annotations and includes annotations for hands, toes and spine. For limb pose read out locations as described in the preceding section, we restrict ourselves to the common minimum joint set between the two, as indicated by the circles in Figure 3.

Training: We start with a Resnet-50-based architecture trained for single person 2D pose estimation on LSP [18, 19] and MPI [2] datasets and use that to initialize the network till *res4f*. We train without the *3DPose* branch on MS-COCO [22] multi-person 2D pose data in accordance with Cao et al.[7]. We then freeze the weights of the core network and the *2DPose+Affinity* branch, and train the *3DPose* branch on our MuCo-3DHP data for 360k iterations with a batch size of 6. More details on the training can be found in the supplementary document.

Loss: The 2D *heatmaps* \mathcal{H}_{COCO} and \mathcal{H}_{MPI} are trained

Table 1. Comparison of our method against the state of the art on single person MPI-INF-3DHP test set. All evaluations use ground-truth bounding box crops around the subject. We report the *Percentage of Correct Keypoints measure in 3D (@150mm)*, and the Area Under the Curve for the same, as proposed by MPI-INF-3DHP. We additionally report the Mean Per Joint Position Error in mm. Higher PCK and AUC is better, and lower MPJPE is better.

Network	Stand/ Walk	Exercise	Sit On	Crouch/ Reach	On the	Sports	Misc.	Total		
	PCK		Chair	PCK	Floor			PCK	PCK	AUC
VNect [26]	87.7	77.4	74.7	72.9	51.3	83.3	80.1	76.6	40.4	124.7
LCR-net [36]	70.5	56.3	58.5	69.4	39.6	57.7	57.6	59.7	27.6	158.4
Zhou et al.[50]	-	-	-	-	-	-	-	69.2	32.5	-
Mehta et al.[25]	86.6	75.3	74.8	73.7	52.2	82.1	77.5	75.7	39.3	117.6
Ours (Torso)	73.7	64.3	65.3	67.3	43.7	69.5	59.5	63.7	31.1	147.1
Ours (Full)	82.2	73.1	76.0	75.8	49.8	78.6	70.6	73.0	36.2	126.2

with per pixel $L2$ loss comparing the predictions to the reference which has unit peak Gaussians with a limited support at the ground truth 2D joint locations, as is common. The *part affinity fields* \mathcal{A}_{COCO} are similarly trained with a per pixel $L2$ loss, using the framework made available by Cao et al. [7]. In order to support the pose inference process described in Section 4.2, the training loss enforced on the *location maps* differs from that of [26]. Per joint type, for all subjects in the scene, a per-pixel $L2$ loss is enforced in the neighborhood of all the 2D joint locations where a 3D pose readout for this particular joint should be possible. The loss is weighted by a Gaussian with limited support centered at the 2D joint location.

5. Results

We demonstrate the merits of our proposed approach through a series of experiments on the single person MPI-INF-3DHP [25] test-set, as well as the proposed multi-person 3D pose test set. We show that our method is significantly more accurate than existing multi-person 3D pose estimation approaches, while being comparable to the state of the art for single person pose estimation. We also use the experiments to establish the usefulness of the proposed multi-person 3D pose test set.

5.1. Ablative Analysis

Torso Only Readout vs. Full Readout: To rule out other confounding factors, we use the single person MPI-INF-3DHP test set to conclusively show the benefit of our 3D pose inference method over naive torso centered pose read out. Pose read out at the torso without further limb based refinement performs significantly worse (63.7 PCK) than our full readout method (73 PCK), as shown in Table 1, and the performance improvement is consistent across activity classes.

Robustness to Occlusion: To test the robustness to occlusion of our approach, we qualitatively evaluate it on the

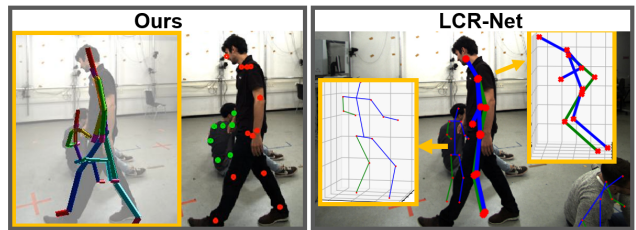


Figure 8. Qualitative comparison of LCR-net [36] and our method for overlap between people.

TS1 sequence of MPI-INF-3DHP overlaid with random textured boxes. Our approach performs well, producing plausible poses even under significant occlusion, and does not exhibit drastic failures which VNect [26] suffers from. LCR-net [36] is also trained to produce plausible poses under occlusion. See Figure 6. Please refer to the supplementary video for more results.

5.2. Comparison with 3D Multi-Person Methods

We report the results of extensive qualitative and quantitative comparisons with the only other known monocular multi-person 3D pose estimation approach of Rogez et al. [36]. For fairness of comparison, in all evaluations we retarget the predictions from LCR-net on to a skeleton with bone-lengths matching the ground truth.

Performance for Single-person Pose Estimation: While LCR-net can handle multiple people in the scene and produces plausible poses under significant occlusion, it suffers from low accuracy on account of its seeming tendency to be conservative about the extent of articulation of the prediction. We show an example in Figure 7.

As show in Table 1, on MPI-INF-3DHP single person test set, LCR-net shows 59.7 PCK, and tends to perform worse than all methods that report their performance on the test set, performing even worse than our torso-only readout (63.7 PCK). Our full method at 73.0 PCK, though slightly worse than the state-of-the-art methods overall, improves over the state of the art on activity classes such as 'Sit on



Figure 9. Visualization of predictions from our method for frames from our multi-person 3D pose test set. Our method can handle strong occlusions (green box on the left), but occlusions where neck and pelvis detections both fail result in people not being detected (red box). Mild limb pose failures are shown on the right (yellow boxes).

Chair’ and ‘Crouch/Reach’ which exhibit significant occlusion (both self occlusions and by a chair).

Performance for Multi-person Pose Estimation: We compare LCR-net and our method on the 20 sequences of our new multi-person 3D pose test set. Since there can be more or fewer predictions per frame than the number of annotated subjects for the frame, on account of people in the background or significant occlusion of one of the main subjects, we use 2D predictions associated with each 3D prediction to find a matching to the annotated subjects in the scene. Figure 10 reports the PCK metric for each each sequence. Our method performs significantly better than LCR-net for most sequences, while being comparable for a few. Our method has a total PCK of 63.7, which is significantly better than the PCK of 51.5 obtained with LCR-net. We provide a joint-wise breakdown of the overall accuracy in the supplementary document.

We also compute the fraction of annotated subjects that were matched to a prediction, which is affected both by the 2D pose prediction quality as well as the method being able to detect a person under severe occlusion. With LCR-net, 82.5% of the annotated subjects were matched, while with our approach, 89% of the annotated subjects were matched.

Figure 8 shows a qualitative comparison of predictions on a frame from the test set showing significant occlusion for the subject in the back. LCR-net fails to estimate the leg articulation for the person in front while predicting a standing pose for the person at the back.

Limitations and Future Work: While our method works well for significant occlusions, it still fails when similar limbs of different persons are in close proximity leading to association ambiguity. Furthermore, we have shown ac-

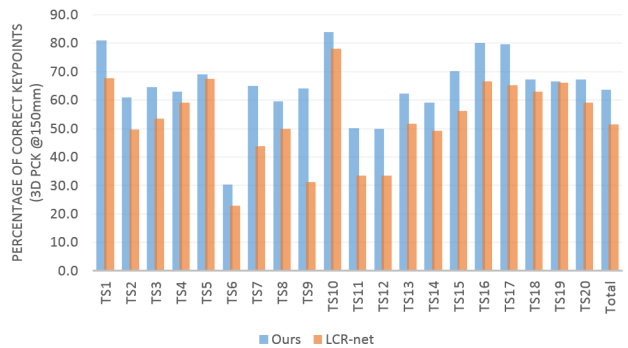


Figure 10. Sequence-wise evaluation of our method and LCR-net[36] on our proposed multi-person 3D pose test set. Our method (in blue) shows significantly better performance than LCR-net (in orange) across all tested sequences.

curate root-relative 3D pose estimation, but estimating the relative sizes of people is challenging and remains an open problem for future work.

6. Conclusion

Multi-person 3D pose estimation from monocular RGB is a challenging problem which has not been addressed extensively by previous work. Our proposed method uses a novel formulation, which is occlusion-robust and scales well with the number of people, in order to reliably estimate the 3D pose even under strong inter-person occlusions. Our method is trained on a new annotated multi-person dataset which was created using a compositing approach leveraging existing single person 3D data. To evaluate our method, we introduce the first real 3D annotated multi-person test set on which we significantly outperform the state of the art.

Supplementary Document: Single-Shot Multi-Person 3D Body Pose Estimation From Monocular RGB Input

1. Network Details

1.1. Architecture

A visualization our network architecture using the web-based visualization tool *Netscope* can be found at <http://ethereon.github.io/netscope/#/gist/069a592125c78fbdd6eb11fd45306fa0>.

1.2. Data

We use 12 out of the 14 available camera viewpoints (using only 1 of the 3 available top down views) in MPI-INF-3DHP [25] training set, and create 400k composite frames of MuCo-3DHP, of which half are without appearance augmentation. For training, we crop around the subject closest to the camera, and apply rotation, scale, and bounding-box jitter augmentation. Since the data was originally captured in a relatively restricted space, the likelihood of there being multiple people visible in the crop around the main person is high. The combination of scale augmentation, bounding-box jitter, and cropping around the subject closest to the camera results in many examples with truncation from the frame boundary, in addition to the inter-person occlusions occurring naturally due to the compositing.

1.3. Training

We train our network using the Caffe [17] framework. The core network’s weights were initialized with those trained for 2D body pose estimation on MPI [2] and LSP [18, 19] datasets as done in [25]. The core network and the *2DPose + Affinity* branch are trained for multi-person 2D pose estimation using the framework provided by Cao et al. [7]. We use the AdaDelta solver, with a momentum of 0.9 and weight decay multiplier of 0.005, and a batch size of 8. We train for 640k iterations with a cyclical learning rate ranging from 0.1 to 0.000005.

The *3DPose* branch is trained with the core network and *2DPose + Affinity* branch weights frozen. We use a batch size of 6 and train for 360k iterations with a cyclical learning rate ranging from 0.1 to 0.000001.

2. Joint-wise Analysis

Figure 1 shows joint-wise accuracy comparison of our approach with LCR-net [36] on the single person MPI-INF-3DHP test set. For limb joints (elbow, wrist, knee, ankle) LCR-net performs comparably or better than our torso-only readout, but our full readout performs significantly better.

Figure 2 shows joint-wise accuracy comparison of our approach with LCR-net on our proposed multi-person 3D

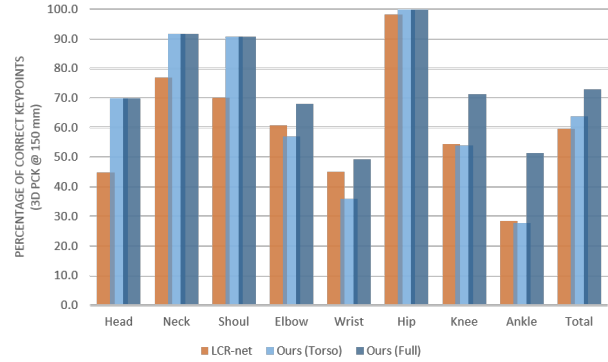


Figure 1. Joint-wise accuracy comparison of our method and LCR-net [36] on the single person MPI-INF-3DHP test set. LCR-net predictions were mapped to the ground truth bone lengths for fairness of comparison.

pose test set. We see that our approach obtains a better accuracy for all joint types for most sequences, only performing worse than LCR-net for a select few joint types on certain sequences (TestSeq18,19,20).

References

- [1] I. Akhter and M. J. Black. Pose-conditioned joint angle limits for 3d human pose reconstruction. In *IEEE Conference on Computer Vision and Pattern Recognition (CVPR)*, pages 1446–1455, 2015.
- [2] M. Andriluka, L. Pishchulin, P. Gehler, and B. Schiele. 2D Human Pose Estimation: New Benchmark and State of the Art Analysis. In *IEEE Conference on Computer Vision and Pattern Recognition (CVPR)*, June 2014.
- [3] M. Andriluka, S. Roth, and B. Schiele. Pictorial structures revisited: People detection and articulated pose estimation. In *IEEE Conference on Computer Vision and Pattern Recognition (CVPR)*, pages 1014–1021, 2009.
- [4] L. Bo and C. Sminchisescu. Twin gaussian processes for structured prediction. In *International Journal of Computer Vision*, 2010.
- [5] F. Bogo, A. Kanazawa, C. Lassner, P. Gehler, J. Romero, and M. J. Black. Keep it SMPL: Automatic estimation of 3D human pose and shape from a single image. In *European Conference on Computer Vision (ECCV)*, 2016.
- [6] A. Bulat and G. Tzimiropoulos. Human pose estimation via convolutional part heatmap regression. In *European Conference on Computer Vision (ECCV)*, 2016.
- [7] Z. Cao, T. Simon, S. Wei, and Y. Sheikh. Realtime multi-person 2d pose estimation using part affinity fields. In *IEEE Conference on Computer Vision and Pattern Recognition (CVPR)*, 2017.
- [8] C.-H. Chen and D. Ramanan. 3d human pose estimation = 2d pose estimation + matching. In *CVPR 2017-IEEE Conference on Computer Vision & Pattern Recognition*, 2017.
- [9] X. Chen and A. L. Yuille. Articulated pose estimation by a graphical model with image dependent pairwise relations. In *Advances in Neural Information Processing Systems (NIPS)*, pages 1736–1744, 2014.

	Ours									LCR-net									Difference								
	Head	Neck	Shoul	Elbow	Wrist	Hip	Knee	Ankle	Total	Head	Neck	Shoul	Elbow	Wrist	Hip	Knee	Ankle	Total	Head	Neck	Shoul	Elbow	Wrist	Hip	Knee	Ankle	Total
TestSeq1	96.8	100.0	96.6	78.0	50.9	99.8	81.0	62.3	81.0	72.4	81.1	73.3	61.1	41.8	94.0	72.8	46.1	66.5	24.4	18.9	23.4	16.9	9.1	5.7	8.2	16.2	14.4
TestSeq2	63.9	85.9	68.3	54.9	47.6	82.4	55.3	42.8	60.9	52.0	66.7	52.9	42.4	31.2	66.9	46.7	37.5	48.2	12.0	19.1	15.4	12.5	16.4	15.4	8.6	5.3	12.7
TestSeq3	79.9	91.9	90.5	56.5	46.8	99.1	42.0	30.2	64.4	64.6	72.3	53.9	32.8	28.8	85.0	44.5	26.4	48.5	15.3	19.6	36.6	23.7	18.0	14.1	-2.4	3.9	15.9
TestSeq4	73.1	82.7	76.5	56.6	49.3	98.5	50.7	31.4	63.0	56.5	79.6	62.4	54.4	47.7	93.2	51.2	30.9	58.2	16.6	3.2	14.1	2.2	1.6	5.3	-0.5	0.5	4.7
TestSeq5	56.5	82.0	79.7	66.2	65.7	93.4	67.3	42.0	69.1	68.0	84.9	72.0	70.4	60.4	84.5	65.0	43.1	67.4	-11.5	-2.9	7.7	-4.2	5.3	8.9	2.3	-1.1	1.7
TestSeq6	6.5	32.1	35.5	12.7	10.9	99.4	23.3	10.8	30.3	6.3	25.9	18.3	16.3	11.9	73.4	7.7	2.3	20.8	0.2	6.2	17.2	-3.6	-1.0	26.1	15.7	8.5	9.5
TestSeq7	66.6	97.8	81.5	47.0	21.0	98.8	63.0	61.9	65.0	34.4	66.7	38.8	31.5	22.9	87.5	49.1	25.6	43.7	32.2	31.0	42.7	15.5	-1.8	11.2	13.8	36.3	21.3
TestSeq8	55.2	71.6	65.8	57.2	45.2	98.5	44.4	42.8	59.6	54.6	68.5	51.2	43.7	34.3	68.2	46.7	31.6	48.2	0.5	3.1	14.6	13.5	10.8	30.3	-2.3	11.2	11.4
TestSeq9	67.2	84.1	81.5	30.1	25.7	100.0	62.7	73.1	64.1	34.9	41.9	34.1	20.0	15.9	45.1	32.8	31.4	31.1	32.2	42.2	47.4	10.2	9.8	54.9	29.8	41.6	33.0
TestSeq10	98.2	100.0	100.0	63.2	52.1	100.0	95.4	77.8	83.9	80.5	97.6	98.0	53.1	31.9	100.0	87.0	87.9	78.1	17.7	2.4	2.0	10.2	20.2	0.0	8.5	-10.2	5.8
TestSeq11	44.0	61.8	56.0	37.3	29.4	96.8	49.2	29.2	50.1	15.5	28.7	26.2	41.0	29.4	58.8	38.3	18.2	33.4	28.4	33.1	29.8	-3.7	0.0	38.0	10.9	11.0	16.7
TestSeq12	30.3	47.9	50.0	48.2	43.8	99.3	42.3	26.8	49.9	15.9	27.3	25.8	40.1	42.7	63.8	27.1	13.5	33.5	14.4	20.7	24.2	8.1	1.1	35.5	15.2	13.3	16.4
TestSeq13	58.5	77.9	74.5	48.6	38.5	96.2	68.9	41.3	62.3	41.7	62.0	51.2	48.0	37.2	78.5	56.9	36.4	51.5	16.7	15.9	23.3	0.5	1.3	17.7	12.0	4.8	10.9
TestSeq14	47.5	73.3	69.7	43.8	38.4	98.7	62.1	41.0	59.2	36.6	63.2	50.7	39.9	29.2	80.7	57.5	37.4	49.3	10.9	10.2	19.0	3.8	9.3	18.0	4.6	3.6	9.8
TestSeq15	62.3	91.2	84.7	58.3	42.6	98.8	77.4	52.3	70.1	39.0	72.2	59.0	44.6	34.4	91.0	73.4	34.3	56.0	23.3	19.0	25.7	13.8	8.2	7.8	3.9	18.0	14.1
TestSeq16	72.9	87.8	86.1	82.3	80.1	97.3	81.9	51.9	80.0	47.8	67.9	65.1	78.7	68.5	93.2	66.9	35.3	66.5	25.1	19.9	21.0	3.6	11.5	4.1	15.0	16.5	13.5
TestSeq17	74.4	73.8	78.0	78.1	61.3	96.5	91.0	78.6	79.6	44.1	77.7	75.7	68.8	58.9	85.4	59.7	46.8	65.2	30.3	-3.9	2.2	9.3	2.3	21.1	31.3	31.7	14.5
TestSeq18	54.8	73.8	77.1	73.1	44.2	96.0	74.6	41.5	67.3	53.7	89.9	83.7	63.9	42.5	89.9	60.8	28.7	63.1	1.1	-16.1	-6.6	9.3	1.7	6.1	13.8	12.8	4.2
TestSeq19	44.9	78.4	79.4	55.2	54.1	100.0	77.7	37.9	66.6	69.5	79.7	67.2	62.5	53.1	81.2	73.9	50.2	66.1	-24.5	-1.3	12.3	-7.3	1.0	18.8	3.8	-12.3	0.5
TestSeq20	50.8	73.5	71.7	62.5	58.6	99.1	69.0	47.5	67.2	70.5	48.8	49.5	67.3	61.9	72.6	64.4	38.0	59.1	-19.6	24.7	22.1	-4.9	-3.3	26.5	4.6	9.5	8.2

Figure 2. Comparison of our method and LCR-net [36] on our proposed multi-person test set, here visualized as joint-wise breakdown of PCK for all 20 sequences, as well as the difference in accuracy between our method and LCR-net. LCR-net predictions were mapped to the ground truth bone lengths for fairness of comparison.

[10] A. Elhayek, E. Aguiar, A. Jain, J. Tompson, L. Pishchulin, M. Andriluka, C. Bregler, B. Schiele, and C. Theobalt. MARCO_nI - ConvNet-based MARKer-less Motion Capture in Outdoor and Indoor Scenes. *IEEE Transactions on Pattern Analysis and Machine Intelligence (PAMI)*, 2016.

[11] G. Gkioxari, B. Hariharan, R. Girshick, and J. Malik. Using k-poselets for detecting people and localizing their keypoints. In *Proceedings of the IEEE Conference on Computer Vision and Pattern Recognition*, pages 3582–3589, 2014.

[12] K. He, X. Zhang, S. Ren, and J. Sun. Deep residual learning for image recognition. In *IEEE Conference on Computer Vision and Pattern Recognition (CVPR)*, 2016.

[13] E. Insafutdinov, M. Andriluka, L. Pishchulin, S. Tang, E. Levinkov, B. Andres, B. Schiele, and S. I. Campus. Art-track: Articulated multi-person tracking in the wild. In *Proc. of CVPR*, 2017.

[14] C. Ionescu, D. Papava, V. Olaru, and C. Sminchisescu. Human3.6m: Large scale datasets and predictive methods for 3d human sensing in natural environments. *IEEE Transactions on Pattern Analysis and Machine Intelligence (PAMI)*, 36(7):1325–1339, 2014.

[15] U. Iqbal and J. Gall. Multi-person pose estimation with local joint-to-person associations. In *European Conference on Computer Vision Workshops*, pages 627–642. Springer, 2016.

[16] E. Jahangiri and A. L. Yuille. Generating multiple diverse hypotheses for human 3d pose consistent with 2d joint detections. In *IEEE International Conference on Computer Vision (ICCV) Workshops (PeopleCap)*, 2017.

[17] Y. Jia, E. Shelhamer, J. Donahue, S. Karayev, J. Long, R. Girshick, S. Guadarrama, and T. Darrell. Caffe: Convolutional architecture for fast feature embedding. In *Proceedings of the 22nd ACM International Conference on Multimedia*, pages 675–678, 2014.

[18] S. Johnson and M. Everingham. Clustered pose and nonlinear appearance models for human pose estimation. In *British Machine Vision Conference (BMVC)*, 2010. doi:10.5244/C.24.12.

[19] S. Johnson and M. Everingham. Learning effective human pose estimation from inaccurate annotation. In *Proceedings of IEEE Conference on Computer Vision and Pattern Recognition*, 2011.

[20] C. Lassner, J. Romero, M. Kiefel, F. Bogo, M. J. Black, and P. V. Gehler. Unite the people: Closing the loop between 3d and 2d human representations. In *IEEE Conf. on Computer Vision and Pattern Recognition (CVPR)*, July 2017.

[21] S. Li, W. Zhang, and A. B. Chan. Maximum-margin structured learning with deep networks for 3d human pose estimation. In *IEEE International Conference on Computer Vision (ICCV)*, pages 2848–2856, 2015.

[22] T.-Y. Lin, M. Maire, S. Belongie, J. Hays, P. Perona, D. Ramanan, P. Dollár, and C. L. Zitnick. Microsoft coco: Common objects in context. In *European conference on computer vision*, pages 740–755. Springer, 2014.

[23] M. Loper, N. Mahmood, J. Romero, G. Pons-Moll, and M. J. Black. SMPL: A skinned multi-person linear model. *ACM Trans. Graphics (Proc. SIGGRAPH Asia)*, 34(6):248:1–248:16, Oct. 2015.

[24] J. Martinez, R. Hossain, J. Romero, and J. J. Little. A simple yet effective baseline for 3d human pose estimation. In *IEEE International Conference on Computer Vision (ICCV)*, 2017.

[25] D. Mehta, H. Rhodin, D. Casas, P. Fua, O. Sotnychenko, W. Xu, and C. Theobalt. Monocular 3d human pose estimation in the wild using improved cnn supervision. In *3D Vision (3DV), 2017 Fifth International Conference on*, 2017.

[26] D. Mehta, S. Sridhar, O. Sotnychenko, H. Rhodin, M. Shafiei, H.-P. Seidel, W. Xu, D. Casas, and C. Theobalt. Vnect: Real-time 3d human pose estimation with a single rgb camera. volume 36, 2017.

[27] F. Moreno-Noguer. 3d human pose estimation from a single image via distance matrix regression. In *CVPR 2017-IEEE Conference on Computer Vision & Pattern Recognition*, 2017.

[28] A. Newell and J. Deng. Associative embedding: End-to-end learning for joint detection and grouping. In *Advances in Neural Information Processing Systems (NIPS)*, 2017.

- [29] A. Newell, K. Yang, and J. Deng. Stacked hourglass networks for human pose estimation. In *European Conference on Computer Vision (ECCV)*, 2016.
- [30] G. Papandreou, T. Zhu, N. Kanazawa, A. Toshev, J. Tompson, C. Bregler, and K. Murphy. Towards accurate multi-person pose estimation in the wild. *arXiv preprint arXiv:1701.01779*, 2017.
- [31] L. Pishchulin, E. Insafutdinov, S. Tang, B. Andres, M. Andriluka, P. Gehler, and B. Schiele. Deepcut: Joint subset partition and labeling for multi person pose estimation. In *IEEE Conference on Computer Vision and Pattern Recognition (CVPR)*, 2016.
- [32] L. Pishchulin, A. Jain, M. Andriluka, T. Thormählen, and B. Schiele. Articulated people detection and pose estimation: Reshaping the future. In *Conference on Computer Vision and Pattern Recognition (CVPR)*, pages 3178–3185. IEEE, 2012.
- [33] G. Pons-Moll, D. J. Fleet, and B. Rosenhahn. Posebits for monocular human pose estimation. In *IEEE Conference on Computer Vision and Pattern Recognition (CVPR)*, pages 2337–2344, 2014.
- [34] A.-I. Popa, M. Zanfir, and C. Sminchisescu. Deep multi-task architecture for integrated 2d and 3d human sensing. *IEEE Conference on Computer Vision and Pattern Recognition (CVPR)*, 2017.
- [35] S. Ren, K. He, R. Girshick, and J. Sun. Faster r-cnn: Towards real-time object detection with region proposal networks. In *Advances in neural information processing systems*, pages 91–99, 2015.
- [36] G. Rogez, P. Weinzaepfel, and C. Schmid. Lcr-net: Localization-classification-regression for human pose. In *CVPR 2017-IEEE Conference on Computer Vision & Pattern Recognition*, 2017.
- [37] N. Sarafianos, B. Boteanu, B. Ionescu, and I. A. Kakadiaris. 3d human pose estimation: A review of the literature and analysis of covariates. *Computer Vision and Image Understanding*, 152:1–20, 2016.
- [38] L. Sigal, A. O. Balan, and M. J. Black. Humaneva: Synchronized video and motion capture dataset and baseline algorithm for evaluation of articulated human motion. *International Journal of Computer Vision (IJCV)*, 87(1-2):4–27, 2010.
- [39] E. Simo-Serra, A. Quattoni, C. Torras, and F. Moreno-Noguer. A joint model for 2d and 3d pose estimation from a single image. In *Conference on Computer Vision and Pattern Recognition (CVPR)*, pages 3634–3641, 2013.
- [40] T. Simon, H. Joo, I. Matthews, and Y. Sheikh. Hand keypoint detection in single images using multiview bootstrapping. In *IEEE Conference on Computer Vision and Pattern Recognition (CVPR)*, 2017.
- [41] C. Sminchisescu and B. Triggs. Kinematic jump processes for monocular 3d human tracking. In *Computer Vision and Pattern Recognition, 2003. Proceedings. 2003 IEEE Computer Society Conference on*, volume 1, pages I–I. IEEE, 2003.
- [42] M. Sun and S. Savarese. Articulated part-based model for joint object detection and pose estimation. In *IEEE International Conference on Computer Vision*, pages 723–730. IEEE, 2011.
- [43] X. Sun, J. Shang, S. Liang, and Y. Wei. Compositional human pose regression. *arXiv preprint arXiv:1704.00159*, 2017.
- [44] C. J. Taylor. Reconstruction of articulated objects from point correspondences in a single uncalibrated image. In *IEEE Conference on Computer Vision and Pattern Recognition (CVPR)*, volume 1, pages 677–684, 2000.
- [45] B. Tekin, P. Márquez-Neila, M. Salzmann, and P. Fua. Learning to fuse 2d and 3d image cues for monocular body pose estimation. In *IEEE International Conference on Computer Vision (ICCV)*, 2017.
- [46] The Capturey. <http://www.thecapturey.com/>, 2016.
- [47] M. Trumble, A. Gilbert, C. Malleson, A. Hilton, and J. Colomosse. Total capture: 3d human pose estimation fusing video and inertial sensors. In *Proceedings of 28th British Machine Vision Conference*, pages 1–13, 2017.
- [48] T. von Marcard, G. Pons-Moll, and B. Rosenhahn. Human pose estimation from video and imus. *Transactions on Pattern Analysis and Machine Intelligence*, 38(8):1533–1547, Jan. 2016.
- [49] H. Yasin, U. Iqbal, B. Krüger, A. Weber, and J. Gall. A Dual-Source Approach for 3D Pose Estimation from a Single Image. In *Conference on Computer Vision and Pattern Recognition (CVPR)*, 2016.
- [50] X. Zhou, Q. Huang, X. Sun, X. Xue, and Y. Wei. Towards 3d human pose estimation in the wild: A weakly-supervised approach. In *Proceedings of the IEEE Conference on Computer Vision and Pattern Recognition*, pages 398–407, 2017.
- [51] X. Zhou, M. Zhu, S. Leonardos, K. Derpanis, and K. Daniilidis. Sparseness Meets Deepness: 3D Human Pose Estimation from Monocular Video. In *IEEE Conference on Computer Vision and Pattern Recognition (CVPR)*, 2015.